Available online at www.sciencedirect.com
SCIENCE DIRECT®
International Journal of Mass Spectrometry 241 (2005) 305–313
International Journal of Mass Spectrometry
www.elsevier.com/locate/ijms

Thermal decomposition of ethylbenzene cations ($C_8H_{10}^+$): experiments and modeling of falloff curves

Abel I. Fernandez[a,1], A.A. Viggiano[a,*], A.I. Maergoiz[b], J. Troe[b], V.G. Ushakov[b,c]

[a] *Air Force Research Laboratory, Space Vehicles Directorate, 29 Randolph Rd., Hanscom AFB, MA 01731-3010, USA*
[b] *Institute for Physical Chemistry, University of Goettingen, Tammannstrasse 6, D-37077 Goettingen, Germany*
[c] *Institute of Problems of Chemical Physics, Russian Academy of Sciences, 142432 Chernogolovka, Russia*

Received 15 November 2004; accepted 20 December 2004

Abstract

The kinetics of the pyrolysis of the ethylbenzene cation, $C_8H_{10}^+$, has been studied in a turbulent ion flow tube (TIFT) from 623 to 673 K and at pressures from 30 to 250 Torr. The ions were prepared by the charge transfer reaction $O_2^+ + C_8H_{10} \rightarrow O_2 + C_8H_{10}^{+*}$ followed by collisional stabilization and then by thermal decomposition in a nitrogen buffer gas. The thermal decomposition rate constants increased with temperature from about 15 to150 s^{-1}, but did not vary with pressure, indicating the results refer to the high pressure limit. The experimental activation energy, 157.8 kJ mol^{-1}, is similar to the bond energy value, 168.3 (±1.2) kJ mol^{-1}, needed to model the data. Modeling of the system using a statistical adiabatic channel model/classical trajectory (SACM/CT) approach provided complete falloff curves for the dissociation and recombination of ethylbenzene. Similar modeling is also presented for the previously published data on *n*-propylbenzene cations. The temperature and pressure dependences of the rate coefficients for dissociation and recombination in the falloff range are represented in analytical form. The chosen format corresponds to that employed in data compilations for the corresponding neutral reaction systems.

Keywords: Thermal decomposition; $C_8H_{10}^+$; Falloff curves; Turbulent ion flow tube

1. Introduction

It is now generally accepted that reactions of molecular ions and of neutral species should be interpreted by common theoretical methods [1]. The present work illustrates this principle by considering the thermal decomposition of molecular cations. The thermal decomposition processes are important steps in plasma-chemical reaction mechanisms. In order to model such systems, analytical representations of the rate coefficients of the elementary reactions involved are required. The dissociation kinetics of neutral species has been studied extensively; examples of critical evaluations are given in [2–5]. Because there is scarcity of data regarding dissociation of ionic species and their temperature and pressure dependence, more work on the rate coefficients of such processes is needed. The present work addresses this goal; here we describe new experimental studies of the thermal decomposition of ethylbenzene cations ($C_8H_{10}^+$). The results are used to construct full sets of falloff curves of this reaction. Additionally, this is also done for dissociation of *n*-propylbenzene ions, for which experimental data has already been presented [6]. The derived temperature (*T*)- and pressure (*p*)-dependences of the rate coefficients $k(T,p)$ are expressed in the same format as used for thermal decomposition reactions of neutral molecules. It is important that not only the same theoretical models but also the same formats of data representation are used in these two areas of kinetics.

Our experimental method employs the charge transfer/chemical activation/collisional stabilization sequence exploited previously [6–8]. This allows the ions to be prepared

* Corresponding author. Tel.: +1 7813772109; fax: +1 7813777091.
E-mail address: albert.viggiano@hanscom.af.mil (A.A. Viggiano).
[1] National Academy of Sciences postdoctoral research fellow.

1387-3806/$ – see front matter © 2004 Elsevier B.V. All rights reserved.
doi:10.1016/j.ijms.2004.12.031

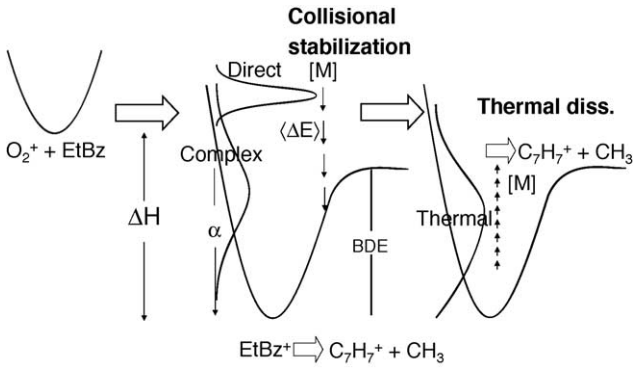

Fig. 1. Schematic energy diagram of charge transfer, competition between collisional stabilization with buffer gas M (α) and unimolecular decomposition (1-α), and subsequent thermal decomposition (pyrolysis).

cleanly in a high temperature environment. In the present case, ethylbenzene cations are formed by the sequence

$$O_2^+ + C_8H_{10} \rightarrow O_2 + C_8H_{10}^{+*} \quad (1)$$

$$C_8H_{10}^{+*} \rightarrow C_7H_7^+ + CH_3 \quad (2)$$

$$C_8H_{10}^{+*} + M \rightarrow C_8H_{10}^+ + M \quad (3)$$

$$C_8H_{10}^+ + M \rightarrow C_8H_{10}^{+*} + M \quad (4)$$

where the asterisk indicates vibrational excitation. Fig. 1 illustrates this reaction scheme. Partial fragmentation of $C_8H_{10}^{+*}$, which is formed from the charge transfer (1), occurs in process (2) in competition with collisional stabilization (3). At lower temperatures, the system is characterized solely by this chemical activation scheme. At temperatures greater than 573 K [8] and at sufficiently high pressures, a fraction of the stabilized $C_8H_{10}^+$ thermally decomposes. This proceeds through collisional reactivation (4) and subsequent dissociation (2) on a slower time scale than the chemical activation sequence.

As the rate coefficients $k(T,p)$ of the pyrolysis depend on T and p, it appears essential to change the experimental variables over wide ranges. Our turbulent ion flow tube (TIFT) can reach both high temperatures and high pressures. This experimental tool has been described previously and used to study energy transfer for excited *n*-propylbenzene [6] and ethylbenzene cations [7] as well as other systems [8–12]. The rate coefficients $k(T,p)$, symbolically represented by

$$k(T,[M]) = \frac{k_4[M]\,k_2}{(k_2 + k_3\,[M])} = k_5, \quad (5)$$

are found to be close to the high pressure limit of the reaction, i.e., $k(T,[M] \rightarrow \infty) = k_{diss,\infty} = k_2\,k_4/k_3$. The rate constant $k_{diss,\infty}$ then can be related to specific rate constants $k(E,J)$ of the dissociation represented here by k_2. We have established this relationship previously [13] accounting in detail for both the E- and J-dependences of $k(E,J)$. Using this relationship, measurements of specific and thermally averaged rate constants, $k(E,J)$ and $k_{diss,\infty}$ respectively, were put on a common basis and analyzed consistently.

Combining the information on $k(E,J)$ with additional information on collisional energy transfer, such as obtained, e.g., from chemical activation studies, the limiting low pressure rate coefficients $k(T,[M] \rightarrow 0) = k_{diss,0} = k_4[M]$ and complete sets of falloff curves of $k(T,[M])$ can be constructed by standard unimolecular reaction theory. We employ the approach from [14] because it has led to simplified expressions for $k(T,[M])$ which have found wide use in representing the kinetics of neutral reactions [2–5]. Following our earlier studies of the reactions $NH_4^+ + NH_3$ (+M) $\rightarrow N_2H_7^+$ (+M) ([15]) and $N_2^+ + N_2$ (+M) $\rightarrow N_4^+$ (+M) ([16]), we extend the application to the organic ions discussed above. $k(T,[M])$ then is represented by the low pressure ($k_{diss,0}$ or $k_{rec,0}$) and high pressure ($k_{diss,\infty}$ or $k_{rec,\infty}$) rate coefficients connected by an approximate interpolation expression which is characterized by a center-broadening factor F_c [14]. Ultimately, data evaluations for dissociations of molecular ions should be performed with respect to these three quantities.

This work also addresses some practical issues regarding combustion. There is interest in the design of advanced hydrocarbon-fueled, hypersonic, airbreathing propulsion systems [17–21]. Because these systems operate on very short time scales, the acceleration of combustion is highly desirable. It has been found that the introduction of plasmas can enhance the rate of combustion [9,22–27]. The ionization enhances combustion, in part, by a reduction of ignition delays which, in turn, are due to the initial fragmentation of fuel molecules. Neutral aliphatics and alkylbenzenes have been used as components in jet fuel surrogate blends for computational modeling of combustion [28–30]. Our group studied the use of ethylbenzene as a fuel surrogate and the kinetics of charge transfer reactions of this compound with air ions for the modeling of plasma-assisted combustion [7,8,12,23,31]. However, accurate kinetic data on the pyrolysis of ethylbenzene cation are lacking. This work combines experimental measurements with theoretical modeling of the fragmentation for this reaction.

The analysis of the reaction can be done in a particularly systematic manner, since separate information is available on collisional energy transfer and on specific rate constants $k(E,J)$, such as required for the full construction of the thermal rate coefficients $k(T,p)$. On this basis, one can demonstrate that falloff curves for the dissociation of neutral and ionic molecules indeed can and should be represented in the same format as used in data evaluations of neutral reactions in atmospheric and combustion chemistry.

2. Experiment

2.1. Experimental technique

Our experiments were conducted in the AFRL turbulent ion flow tube (TIFT) which previously has been described in detail [8,10] such that the technique is only briefly summarized here. The TIFT is similar to low-pressure flow tubes

except that larger flow rates are used to achieve higher pressures and Reynolds numbers. The O_2^+ precursor ions were created upstream by flowing a mixture of a few percent of O_2 diluted in Ar through an off-axis corona discharge source; the low [O_2] prevented unwanted side reactions and the falsification [32,33] of pyrolysis rate constant measurements. The ions flowed through a small orifice into a sidearm and were entrained by a large flow of nitrogen buffer gas (from liquid). The gas mixture entered the flow tube where the neutral reagent was injected through a moveable on-axis tube. At the end of the flow tube, most of the gas was removed by a large mechanical pump; a small fraction was sampled through a truncated nosecone orifice (150 μm diameter). The core of the supersonic expansion, occurring downstream of the orifice, was sampled through a skimmer into a quadrupole mass spectrometer which acted as a mass selector. The resulting ions were subsequently counted by a discrete dynode electron multiplier.

In order to elevate the temperature, six zones of heating were used and maintained to ±2 K by Watlow heating controllers. The main flow tube was heated in four zones, two short zones at both ends, a long middle section, and a zone inside the vacuum chamber just upstream of the nosecone. The connection between the corona discharge tube and the sidearm was also heated. Lastly, it was found that preheating of the buffer gas is needed. During the course of this work, the preheater design was changed to allow for higher temperatures. The new preheater consisted of two Mellen split type (clam shell) tubular heating elements that surrounded a tubular piece of copper or stainless steel; the gas flowed through narrow channels (which traverse the tube along the axis) that have a radial-spoke cross-section. The pattern was chosen to promote efficient heating.

As in our earlier work [8], the $C_8H_{10}^+$ was prepared by collisional charge transfer with the O_2^+ precursor; this occurred downstream of the moveable injector. In the absence of ethylbenzene, the O_2^+ signal was dominant. Common impurities were $H_3O^+(H_2O)_{0,1}$ and $O_2^+(H_2O)$. Since the relative concentrations of the impurities were less than 2%, corrections [34] to the recorded branching ratios were only small. When ethylbenzene was added, ions at 91, 92, 106, and 119 a.m.u. were observed. The high mass peak corresponded to secondary reactions of the aromatic benzylium ($C_7H_7^+$), $m/z = 91$, with neutral ethylbenzene [35]. The peak at 92 a.m.u. was small and hidden in the adjacent 91 a.m.u. signal unless higher resolution spectra were used to separate the two peaks. An isotope correction was made.

The experimental procedure for determining the thermal decomposition rate coefficients was identical to that of our earlier study [6] of $C_9H_{12}^+$ (propylbenzene) pyrolysis and was summarized here. Branching ratios of the ion products were recorded, varying the concentration of the neutral reagent by varying its flow rate while all other conditions were kept constant. The accurate evaluation required both secondary chemistry and finite flow rates to be accounted for. The former was taken into account by varying [C_8H_{10}] and extrapolating to zero concentration. The accessible pressure range was limited by the small signals at low P and allowable intensity of impurity ions at high P. Thermal decomposition of $C_8H_{10}^+$ is slow below 573 K [8] and the current upper temperature limit of the TIFT is limited to about 673 K.

A steady-state solution of the kinetics Eqs. (1)–(4) yielded,

$$\frac{S}{D} \approx \frac{k_3[\mathrm{M}]/k_2\left[1-\exp(-k_5 t)\right]}{k_5 t(1+k_3[\mathrm{M}]/k_2)-(k_3[\mathrm{M}]/k_2)[1-\exp(-k_5 t)]} \tag{6}$$

with k_5 corresponding to $k(T,[\mathrm{M}])$ from Eq. (5). Minor channels were neglected. Extrapolating to zero time led to $(S/D)_0$, the stabilization-to-decomposition ratio in the absence of thermal decomposition

$$\left(\frac{S}{D}\right)_0 = \frac{\left[C_9H_{12}^+\right]}{\left[C_7H_7^+\right]} = \frac{k_3\,[\mathrm{M}]}{k_2} \tag{7}$$

Substituting Eq. (7) into Eq. (6) yielded

$$\frac{S}{D} \approx \frac{(S/D)_0\left[1-\exp(-k_5 t)\right]}{k_5 t(1+(S/D)_0)-(S/D)_0[1-\exp(-k_5 t)]}. \tag{8}$$

Since data were taken by extrapolating to zero extent of reaction, we made the simplifying assumption that the decrease of the product of concentrations of [C_8H_{10}] and [O_2^+] during the course of the reaction was insignificant. The extrapolation along with small changes in S/D at low temperatures and pressure introduced significant scatter in the data which was reduced by replacing the $(S/D)_0$ fitted parameter with a 2-parameter linear expression

$$(S/D)_0 = a_1 + a_2\,[\mathrm{N_2}]. \tag{9}$$

This assumption is reasonable since our earlier results [7,8] indicate that the $(S/D)_0$ versus [M] plots are quasi-linear. Substituting Eq. (9) into Eq. (8) results in a three-parameter expression and all the data at a particular temperature can be fit simultaneously. Nonlinear least squares fits of the time dependence of S/D at each temperature to the three-parameter expression of Eqs. (8) and (9) yielded both k_5 and a line for $(S/D)_0$. Two parameter fits were also made at each temperature and pressure. These lead to approximately the same results for the pyrolysis rate constant but with more scatter. Those fits showed that the rates were independent of pressure within our uncertainty and therefore in the high pressure limit.

The accuracy of the procedure was estimated to be about a factor of 2 at lower temperatures where declines were small and slightly less at higher temperature. Fig. 2 shows a typical time dependence of S/D at $T = 673$ K and at nitrogen buffer pressures of 30, 100, and 250 Torr. The three parameter fit is shown as lines.

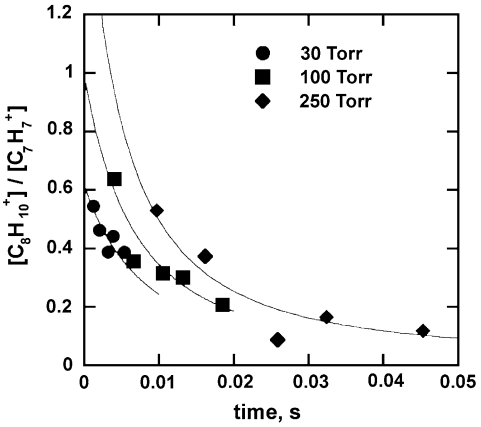

Fig. 2. Thermal decomposition of $C_8H_{10}^+$ at 673 K. $[C_8H_{10}^+]/[C_7H_7^+] = S/D$ is plotted vs reaction time at pressures of 30 (●), 100 (■), and 250 (♦) Torr of nitrogen. Best fits to Eqs. (8) and (9), shown as curves, yield values of $(S/D)_0$, the ratio of stabilization to dissociation in the absence of thermal decomposition, and k_5, the first-order thermal decomposition rate coefficient of $C_8H_{10}^+$.

2.2. Experimental results

The pyrolysis of ethylbenzene cations was studied at temperatures of 623, 648, and 673 K. Pressure of the N_2 buffer gas was varied from 30 to 250 Torr. These measurements extend considerably the temperature range of the earlier unimolecular decomposition data for this ion [7,8] which were performed at 423, 473, and 523 K; these did not exhibit thermal decomposition.

The raw data, such as those in Fig. 2, were fitted to Eqs. (8) and (9). Table 1 compares the resulting slopes of $(S/D)_0$ versus $[N_2]$ with the data from [7]. As expected, the pyrolysis data exhibit smaller slopes because a higher buffer gas temperature will lead to less stabilization of the excited charge transfer product, i.e., reaction (3) is slower. However, the 673 K data have a somewhat greater slope than those of the 623 and 648 K data for unknown reasons. Moreover, while a_1-values in [7] were scattered around $a_1 = 0.7$, the present values seem to be somewhat smaller but their scatter is too large for definitive conclusions. The a_1-values increase with decreasing temperature which was interpreted quantitatively in [7]. We did not repeat this analysis for the present data since, apart from some scatter, the present average value of a_2 follows the trends of the measurements from lower temperatures.

Table 1
Stern-Volmer quenching parameters a_1 and a_2 in Eq. (9) and pyrolysis rate constants k_5

T (K)	a_1	a_2 (cm^3 molecule^{-1})	k_4 (s^{-1})	Reference
423	0.7	2.7×10^{-18}	–	[7]
473	0.7	2.0×10^{-18}	–	[7]
523	0.6	1.6×10^{-18}	–	[7]
623	0.48	3.5×10^{-19}	15.7	This work
648	0.79	2.6×10^{-19}	51.5	This work
673	0.46	3.8×10^{-19}	151.2	This work

The values of k_5 range increase from 15 to 150 s^{-1} with increasing temperature. The alternative two parameter analysis showed that the rate constants do not vary over the entire pressure domain, within error, which is indicative of the high pressure limit. Our theoretical analysis presented below is in accord with this conclusion. The three parameter analysis yields one fitted value of k_5 at each temperature over the entire number density range which is on the order of 10^{18} molecule cm^{-3}. An Arrhenius plot of the pyrolysis rate constants yields

$$k_5 = 2.7 \times 10^{14} \exp(-157.8\,\text{kJ mol}^{-1}/RT)\,\text{s}^{-1}. \quad (10)$$

This activation energy is on the order of the bond energy $E_0 = 168.3\ (\pm 1.2)$ kJ mol^{-1} as employed in the analysis of [7]. Below we compare this measured k with predictions based on modeling including specific rate constants $k(E,J)$ normalized to experimental data.

3. Modeling of falloff curves

3.1. Limiting high pressure rate coefficients

The absence of a pressure dependence in the measurements of the dissociation rate coefficients as well as the modeling described in the following sections, indicate that the present experimental conditions coincide with the high pressure limit of the reaction. For this reason, we first consider the limiting high pressure rate coefficients $k_{\text{diss},\infty}$. For accurate modeling, one replaces the simple expression, $k_{\text{diss},\infty} = k_2k_4/k_3$, by the more accurate one that includes many states

$$k_{\text{diss},\infty} = \sum_{J=0}^{\infty}(2J+1)\int_{E_0(J)}^{\infty} k(E,J)f(E,J)\,\text{d}E. \quad (11)$$

This expression relates $k_{\text{diss},\infty}$ with the specific rate constants $k(E,J)$ corresponding to k_2 and $f(E,J)$ denotes equilibrium populations corresponding to k_4/k_3. $k(E,J)$ have been measured at selected energies E and over certain distributions of angular momentum, J, for $C_8H_{10}^+$ in [36,37] and for $C_9H_{12}^+$ in [38]. Our measured values for $k_{\text{diss},\infty}$, therefore, should be compared with these measurements of $k(E,J)$. The comparison, however, is much less direct than one might wish: $k_{\text{diss},\infty}$ generally depends more on the values of the bond energy $E_0 = E_0(J=0)$ than $k(E,J)$. In addition, $k_{\text{diss},\infty}$ is averaged over distributions of J in a way that generally differs from that of the $k(E,J)$ measurements. The comparison, therefore, requires a full theoretical modeling both of $k_{\text{diss},\infty}$ and $k(E,J)$.

We have performed this full modeling in [13] using a statistical adiabatic channel model/classical trajectory (SACM/CT) approach on a short-range valence/long-range induced-dipole switching potential. Because the real potential is not available from ab initio calculations, model potentials were employed. The uncertain switching from the

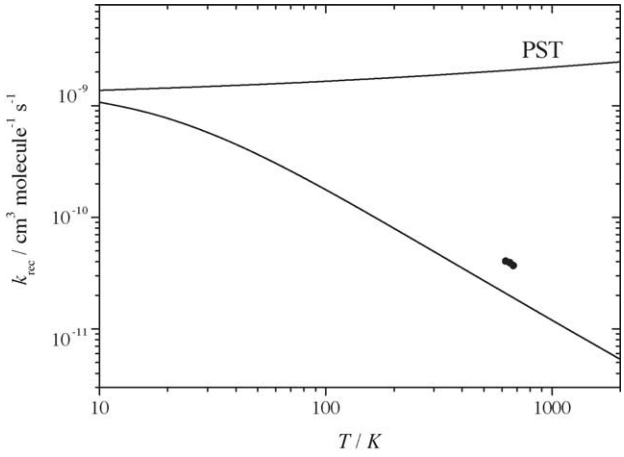

Fig. 3. High pressure rate coefficients $k_{rec,\infty}$ for the reaction $C_7H_7^+ + CH_3 \rightarrow C_8H_{10}^+$ (lines = calculations from [13], PST = phase space theory, lower line = SACM/CT calculations, points = experimental results from this work converted with the equilibrium constant K_c from dissociation data).

pronounced anisotropy of the short-range valence potential to the (nearly) vanishing anisotropy of the long-range electrostatic potential, therefore, was parameterized with a single fit parameter obtained by using the measured $k(E,J)$. On this basis, $k_{diss,\infty}$(T) was predicted in [13]. As shown below, the derived $k_{diss,\infty}$ agree well with the measured values which indicates an internal consistency of the experimental specific and thermal rate constants. In order to reduce the influence from uncertainties in the bond energy $E_0(J)$, we choose a representation of the modeled high pressure recombination rate coefficients $k_{rec,\infty}$ as a function of the temperature. Figs. 3 and 4 show the results for the $C_8H_{10}^+$- and $C_9H_{12}^+$-systems, respectively. The rate coefficients derived with anisotropic potential energy surfaces are compared with values for potentials, whose anisotropies are artificially switched off while the minimum energy path potentials are

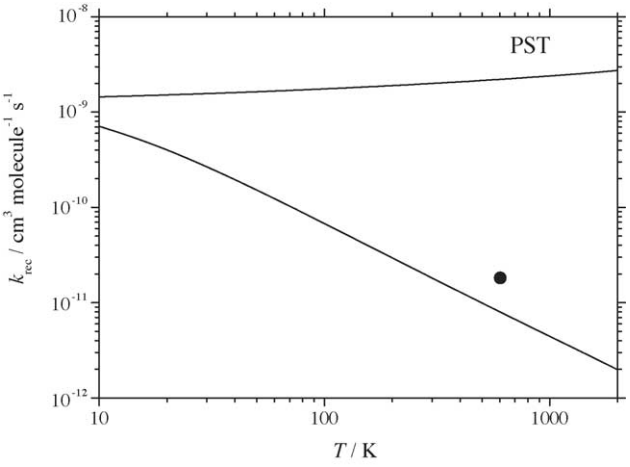

Fig. 4. As Fig. 3 for the reaction $C_7H_7^+ + C_2H_5 \rightarrow C_9H_{12}^+$ (experimental point from [6]).

kept unchanged. The latter corresponds to phase space theory (PST), such as elaborated by Pechukas and Light, Nikitin, Chesnavich and Bowers, and others (see the detailed description in [1]). Our version of PST corresponds closest to the orbiting transition state phase space theory of Chesnavich and Bowers [39,40], however, accounting for the centrifugal barriers along the minimum energy path of the relevant potential energy surface. We observe that $k_{rec,\infty}$ increasingly falls below $k_{rec,\infty}^{PST}$ with increasing T. This effect is due to an increasing shift of the effective bottleneck of the reaction into the more anisotropic range of the potential with increasing thermal energy. The thermal rigidity factors $f_{rigid}(T)$ (see, e.g. [41]) then decrease with increasing temperature. The high pressure recombination rate coefficients of Figs. 3 and 4, over the range 500–1000 K, are approximated by the expressions

$$k_{rec,\infty} \approx 2.3 \times 10^{-11}(T/600\,\mathrm{K})^{-1.2}\,\mathrm{cm^3\,molecule^{-1}\,s^{-1}} \quad (12)$$

for

$$C_7H_7^+ + CH_3 \rightarrow\ C_8H_{10}^+$$

and

$$k_{rec,\infty} \approx 8.0 \times 10^{-12}(T/600\,\mathrm{K})^{-1.1}\,\mathrm{cm^3\,molecule^{-1}\,s^{-1}} \quad (13)$$

for $C_7H_7^+ + C_2H_5 \rightarrow C_9H_{12}^+$. The corresponding dissociation rate coefficients $k_{diss,\infty}$ are obtained from the above expressions and from the equilibrium constants K_c,

$$K_c = \frac{k_{diss,\infty}}{k_{rec,\infty}}, \quad (14)$$

which are modeled consistently with Eqs. (12) and (13) over the range 500–1000 K by

$$K_c = 5.0 \times 10^{25}\,(T/600\,\mathrm{K})^{-0.5} \times \exp(-E_0/kT)\,\mathrm{molecule\,cm^{-3}} \quad (15)$$

with $E_0/k = 20240$ K for the $C_8H_{10}^+$-system and

$$K_c = 1.7 \times 10^{27}(T/600\,\mathrm{K})^{-0.9} \times \exp(-E_0/kT)\,\mathrm{molecule\,cm^{-3}} \quad (16)$$

with $E_0/k = 20070$ K for the $C_9H_{12}^+$-system (for the employed molecular parameters and their origin, see [13]). In this way for $C_8H_{10}^+$,

$$k_{diss,\infty} = 1.2 \times 10^{15}(T/600\,\mathrm{K})^{-1.7}\exp(-E_0/kT)\mathrm{s^{-1}} \quad (17)$$

with $E_0 = 168.3\,\mathrm{kJ\,mol^{-1}}$. Near 650 K, this reduces to

$$k_{diss,\infty} = 1.9 \times 10^{14}\exp(-159.2\,\mathrm{kJ\,mol^{-1}}/RT)\,\mathrm{s^{-1}}. \quad (18)$$

For $C_9H_{12}^+$, the similar expressions are

$$k_{diss,\infty} = 1.4 \times 10^{16}(T/600\,\mathrm{K})^{-2.0}\exp(-E_0/kT)\,\mathrm{s^{-1}} \quad (19)$$

with $E_0 = 166.9\,\mathrm{kJ\,mol^{-1}}$ and

$$k_{\mathrm{diss},\infty} = 1.6 \times 10^{15} \exp(-156.1\,\mathrm{kJ\,mol^{-1}}/RT)\,\mathrm{s^{-1}} \quad (20)$$

near 650 K.

Employing the same equilibrium constants K_c, the values of our measured dissociation rate coefficients k_{diss} for $C_8H_{10}^+$ from this work and for $C_9H_{12}^+$ from [6] are converted into k_{rec} and shown in Figs. 3 and 4 together with the modeled k_{rec}. In both systems, the measurements are less than a factor of two different from the predictions. This is well within the uncertainties of the measurements of $k(E)$ and k_{diss} and of K_c through the calculated reaction entropies and the employed reaction enthalpies. However, before definite conclusions can be drawn, it must be demonstrated that the measured k_{diss} are sufficiently close to the high pressure limiting $k_{\mathrm{diss},\infty}$. Firstly, this requires modeling of limiting low pressure rate coefficients $k_{\mathrm{diss},0}$ and then the falloff curves used to interpolate between the two pressure regimes. This modeling is given in the two following subsections.

3.2. Limiting low pressure rate coefficients

In order to estimate the limiting low pressure rate coefficients $k_{\mathrm{diss},0}$, we employ standard unimolecular rate theory in the formulation of [14], i.e., we write

$$k_{\mathrm{diss},0} = [M]\beta_c Z \left[\frac{\rho_{\mathrm{vib,h}}(E_0)kT}{Q_{\mathrm{vib}}}\right] F_E F_{\mathrm{anh}} F_{\mathrm{rot}} \exp(-E_0 kT). \quad (21)$$

The parameters have been defined in [14] and only the nontrivial factors are discussed in the following. We assume that the collision number Z can be approximated by the Langevin rate constant for ion-induced dipole capture (see, e.g. [42]). The collision efficiency β_c is estimated [43] by

$$\frac{\beta_c}{1-\beta_c^{1/2}} \approx \frac{-\langle\Delta E\rangle}{F_E kT}, \quad (22)$$

where $\langle\Delta E\rangle$ is the average energy transferred per collision. Recently, we have reported $\langle\Delta E\rangle$ in an N_2 buffer as $-\langle\Delta E\rangle/hc = 285\ (\pm 150)\ \mathrm{cm^{-1}}$ for $C_8H_{10}^+$ in [7] and 200 $(\pm 100)\ \mathrm{cm^{-1}}$ for $C_9H_{12}^+$ in [6]. There is some uncertainty in the anharmonicity factor, F_{anh}. We use $F_{\mathrm{anh}} \approx 2.5$ in accord with the approach discussed in [44]; however, the uncertainty of F_{anh} has little relevance to the present work. The estimate of the rotational factor F_{rot} requires information on the centrifugal barriers $E_0(J)$ of the reaction. These are obtained from the minimum energy path potential of the reaction. The calculations from [13] show that $E_0(J)$ approaches the well known expressions for ion-induced dipole potentials at $J \to 0$ while increasing deviations occur with increasing J. With the molecular parameters given in [13], the calculation of $k_{\mathrm{diss},0}$ then is straightforward, leaving most of the remaining uncertainty in the product $\beta_c F_{\mathrm{anh}} F_{\mathrm{rot}}$. We estimate this uncertainty to be about a factor of two, which adds to the uncertainty of E_0 as mentioned previously. For the temperature range 500–1000 K, this treatment gives

$$k_{\mathrm{rec},0} \approx [N_2] 1.3 \times 10^{-23} (T/600\,\mathrm{K})^{-14.2}\,\mathrm{cm^6\,molecule^{-2}\,s^{-1}} \quad (23)$$

for the $C_8H_{10}^+$-system and

$$k_{\mathrm{rec},0} = [N_2] 1.1 \times 10^{-24} (T/600\,\mathrm{K})^{-16.9}\,\mathrm{cm^6\,molecule^{-2}\,s^{-1}} \quad (24)$$

for the $C_9H_{12}^+$-system.

3.3. Falloff curves

Our interpolation between the limiting low pressures (k_0) and high pressure (k_∞) rate coefficients employs the doubly reduced expression

$$\frac{k}{k_\infty} = \left(\frac{k_0/k_\infty}{1+k_0/k_\infty}\right) F(k_0/k_\infty) \quad (25)$$

with the broadening factor $F(k_0/k_\infty)$ from [14]. $F(k_0/k_\infty)$ contains a weak collision contribution $F^{\mathrm{WC}}(k_0/k_\infty)$, which depends on $\langle\Delta E\rangle$ and which was approximated by the method from [14] and a strong collision contribution $F^{\mathrm{SC}}(k_0/k_\infty)$. We have calculated $F^{\mathrm{SC}}(k_0/k_\infty)$ in three ways. First, we have represented the five transitional modes of the reaction by low-frequency oscillators and applied rigid activated complex RRKM theory, such as described in detail in [1]. Second, we have used phase space theory to account for the E- and J-dependence of $k(E,J)$. Finally, we also have accounted for the effects of anisotropy of the potential in our SACM/CT treatment, i.e., included E- and J-specific rigidity factors $f_{\mathrm{rigid}}(E,J)$. The latter two treatments were found to give nearly the same $F^{\mathrm{SC}}(k_0/k_\infty)$. Some differences in the shapes of the broadening factors between RRKM and SACM/CT calculations were found and these are illustrated below.

We present full sets of falloff curves in two ways. First, we show sets of RRKM strong collision falloff curves. Second, we compare strong collision broadening factors from RRKM and SACM/CT calculations. RRKM strong collision curves are presented in Figs. 5 and 6 on the basis of $k_{\mathrm{rec},\infty}$ and $k_{\mathrm{rec},0}$ from Sections 3.1 and 3.2. Figs. 5 and 6 illustrate marked shifts of the falloff curves with changing temperature. While the present experiments (and those of [6]) obviously correspond to conditions near to the high pressure limit, values of k_{rec} below $k_{\mathrm{rec},\infty}$ are expected at higher temperatures for the same [M]. Figs. 5 and 6 illustrate this decay of $k_{\mathrm{rec}}(T\,[\mathrm{M}])$ at fixed [M] with increasing T which partly is due to falloff and partly to the decrease of $k_{\mathrm{rec},\infty}(T)$. $k_{\mathrm{rec},\infty}$

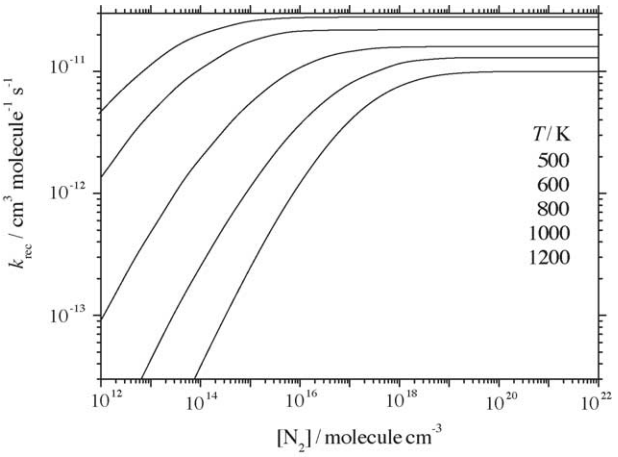

Fig. 5. Falloff curves for the reaction $C_7H_7^+ + CH_3$ (+N_2) → $C_8H_{10}^+$ (+N_2) for T = 500, 600, 800, 1000, and 1200 K (from top to bottom), RRKM strong collision interpolation between $k_{rec,0}$ and $k_{rec,\infty}$, $k_{rec,0}$- and $k_{rec,\infty}$-values from this work, see text).

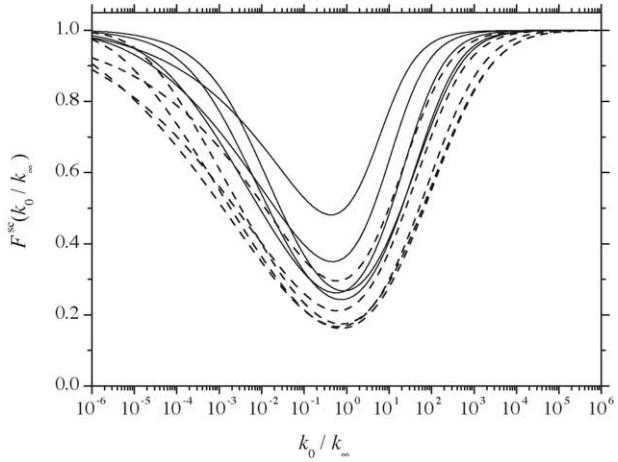

Fig. 7. Strong collision broadening factors $F^{SC}(k_0/k_\infty)$ for the reaction $C_7H_7^+ + CH_3$ (+N_2) → $C_8H_{10}^+$ (+N_2) from SACM/CT calculations (full lines) and RRKM calculatons (dashed lines) (T (K) = 1200, 1000, 800, 500, 600 from top to bottom at k_0/k_∞ = 2).

has a much weaker temperature dependence. One observes a somewhat unusual trend from $C_8H_{10}^+$ to $C_9H_{12}^+$: the centers of the falloff curves $[N_2]_c = k_{rec,\infty}/k_{rec,0}$ at 600 K are equal to $[N_2]_c = 1.7 \times 10^{12}$ molecule cm^{-3} for $C_8H_{10}^+$ and $[N_2]_c = 7.4 \times 10^{12}$ molecule cm^{-3} for $C_9H_{12}^+$. This is opposite to the trend usually observed for increasing molecular complexity. However, because of different reactant frequency patterns $k_{rec,0}$ is larger for $C_8H_{10}^+$ than for $C_9H_{12}^+$. This effect is only partly compensated by a smaller $k_{rec,\infty}$ for $C_9H_{12}^+$ such that the predicted trend results.

Figs. 7 and 8 compare strong collision broadening factors from RRKM and SACM/CT calculations. Although the trends are the same, RRKM calculations give smaller broadening factors than SACM/CT calculations. We do not further elaborate these fine details because weak collision broadening reduces SACM/CT roughly to the strong collision RRKM results. The falloff curves shown in Figs. 5 and 6, therefore, are accurate within an uncertainty of a factor of 2.

3.4. Approximate representation of k(T,[M])

In this section, we provide analytical expressions for the T- and [M]-dependent rate coefficients $k_{rec}(T,[M])$ which, when combined with the equilibrium constants K_c from Eqs. (15) and (16), can be converted into $k_{diss}(T,[M])$. We use $k_{rec,\infty}$ from Eqs. (12) and (13), $k_{rec,0}$ from Eqs. (23) and (24) and the falloff interpolation from Eq. (25). At an acceptable level of approximation, asymmetries of the broadening factors $F(k_0/k_\infty)$ in Eq. (25) are neglected and the simple expression

$$F(x) \approx F_c^{1/\left\{1+[(\log x)/N]^2\right\}} \tag{26}$$

from [14] with $\log x = {}^{10}\log(k_{rec,0}/k_{rec,\infty})$ and $N \approx 0.75$–$1.27\,{}^{10}\log F_c$ is used. The center-broadening factor F_c from 500 to 1000 K was derived from the calculations

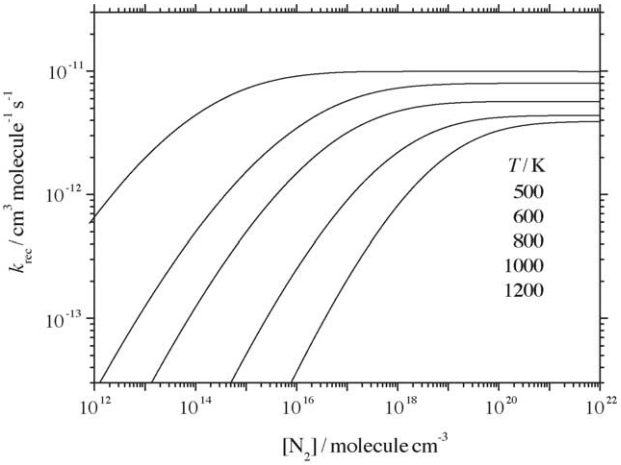

Fig. 6. As Fig. 5 for the reaction $C_7H_7^+ + C_2H_5$ (+N_2) → $C_9H_{12}^+$ (+N_2).

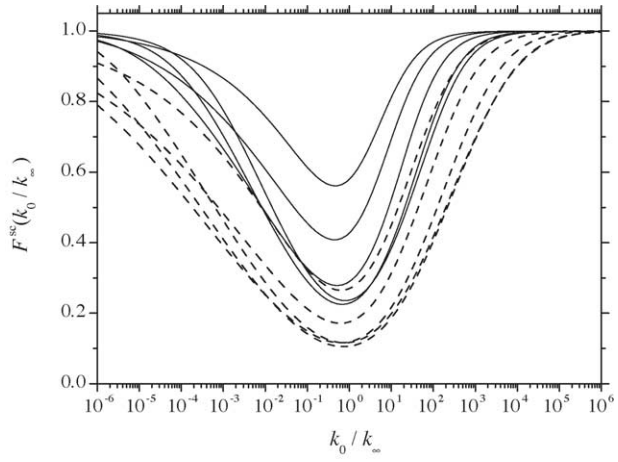

Fig. 8. As Fig. 7 for the reaction $C_7H_7^+ + C_2H_5$ (+N_2) → $C_9H_{12}^+$ (+N_2).

of Section 3.3,

$$F_c(T) \approx 0.25 \pm 0.5 \quad (27)$$

for the $C_8H_{10}^+$-system and

$$F_c(T) \approx 0.23 \pm 0.5 \quad (28)$$

for the $C_9H_{12}^+$-system. F_c is known to decrease with increasing temperature at small T, before it increases at high T [14,45–47]. This temperature range apparently corresponds to the intermediate regime. At the present stage it appears premature to modify Eq. (26) in order to account for the asymmetries of the falloff curves illustrated in Figs. 7 and 8.

4. Summary and conclusions

We have measured thermal dissociation rates for ethylbenzene cations by preparing the ions via a sequence involving charge transfer, chemical activation, and collisional stabilization. There was no apparent pressure dependence of the measured rate coefficients which indicated that the reaction was near the high pressure limit. Modeling of the reaction by unimolecular rate theory provided falloff curves for the dissociation (and the reverse recombination) of ethylbenzene and *n*-propylbenzene cations. The results over the range 500–1000 K were represented by the approximate expressions

$$k_{\mathrm{rec},\infty} \approx 2.3 \times 10^{-11}(T/600\,\mathrm{K})^{-1.2}\,\mathrm{cm^3\,molecule^{-1}\,s^{-1}}$$

$$k_{\mathrm{rec},0} \approx [\mathrm{N_2}]1.3 \times 10^{-23}(T/600\,\mathrm{K})^{-14.2}\,\mathrm{cm^6\,molecule^{-2}\,s^{-1}}$$

$$F_c \approx 0.25 \pm 0.05$$

$$K_c = \frac{k_{\mathrm{diss}}}{k_{\mathrm{rec}}} \approx 5.0\times10^{25}(T/600\,\mathrm{K})^{-0.5}\exp(-E_0/kT)\,\mathrm{molecule\,cm^{-3}}$$

with $E_0 = 168.3\,\mathrm{kJ\,mol^{-1}}$ for the $C_8H_{10}^+$-system and

$$k_{\mathrm{rec},\infty} \approx 8.0 \times 10^{-12}(T/600\,\mathrm{K})^{-1.1}\mathrm{cm^3\,molecule^{-1}\,s^{-1}}$$

$$k_{\mathrm{rec},0} \approx [\mathrm{N_2}]1.1 \times 10^{-24}(T/600\,\mathrm{K})^{-16.9}\,\mathrm{cm^6\,molecule^{-2}\,s^{-1}}$$

$$F_c \approx 0.23 \pm 0.05$$

$$K_c = \frac{k_{\mathrm{diss}}}{k_{\mathrm{rec}}} \approx 1.7\times10^{27}(T/600\,\mathrm{K})^{-0.9}\exp(-E_0/kT)\,\mathrm{molecule\,cm^{-3}}$$

with $E_0 = 166.9\,\mathrm{kJ\,mol^{-1}}$ for the $C_9H_{12}^+$-system. As shown in Figs. 3 and 4, agreement between the modeled and the measured rate coefficients would be obtained, if the preexponential factor of K_c either would be increased by about a factor of 1.8 for the $C_8H_{10}^+$-system (a factor of 2.2 for the $C_9H_{12}^+$-system) or E_0 lowered by about 3.5 kJ mol^{-1}. In doing the former, the following data, based on the dissociation experiments, are the final recommended expressions,

$$k_{\mathrm{diss},\infty} = 3.4 \times 10^{14}\exp(-159.2\,\mathrm{kJ\,mol^{-1}}/RT)\,\mathrm{s^{-1}}$$

$$k_{\mathrm{diss},0} = [\mathrm{N_2}]\,1.2 \times 10^3(T/600\,\mathrm{K})^{-14.7} \times \exp(-E_0/kT)\,\mathrm{cm^3\,molecule^{-1}\,s^{-1}}$$

$$F_c \approx 0.25$$

$$K_c = 9.0 \times 10^{25}(T/600\,\mathrm{K})^{-0.5} \times \exp(-E_0/kT)\,\mathrm{molecule\,cm^{-3}}$$

with $E_0 = 168.3\,\mathrm{kJ\,mol^{-1}}$ for the $C_8H_{10}^+$-system and

$$k_{\mathrm{diss},8} = 3.5 \times 10^{15}\exp(-156.1\,\mathrm{kJ\,mol^{-1}}/RT)\,\mathrm{s^{-1}}$$

$$k_{\mathrm{diss},0} = [\mathrm{N_2}]\,4.1 \times 10^3\,(T/600\,\mathrm{K})^{-17.9} \times \exp(-E_0/kT)\,\mathrm{cm^3\,molecule^{-1}\,s^{-1}}$$

$$F_c \approx 0.23$$

$$K_c = 3.7 \times 10^{27}(T/600\,\mathrm{K})^{-0.9} \times \exp(-E_0/kT)\,\mathrm{molecule\,cm^{-3}}$$

with $E_0 = 166.9\,\mathrm{kJ\,mol^{-1}}$ for the $C_9H_{12}^+$-system. These expressions and the falloff Eqs. (25) and (26) may serve as inputs for data compilations and computer models in a similar manner to those used for neutral reactions. The present treatment also conveniently allows for modifications when more accurate molecular input data become available.

Acknowledgments

The authors have enjoyed many enlightening discussions of various aspects of unimolecular theory and ion-molecule dynamics with W.L. Hase. Financial support of this work from the Deutsche Forschungsgemeinschaft (SFB 357 “Molekulare Mechanismen unimolekularer Reaktionen”), the European Office for Aerospace Research and Development (EOARD Grant No. FA8655-03-1-3034) and the United States Air Force Office of Scientific Research (Project 2303 EP4) is gratefully acknowledged.

References

[1] T. Baer, W.L. Hase, Unimolecular Reaction Dynamics. Theory and Experiment, Oxford University Press, New York, Oxford, 1996.
[2] G.P. Smith, D.M. Golden, M. Frenklach, N.W. Moriarty, B. Eiteneer, M. Goldenberg, C.T. Bowman, R.K. Hanson, S. Song, W.C. Gardiner, V.V. Lissianski, Z. Qin, GRI-Mech. 3.0, 2004. http://me.berkeley.edu/grimech/.
[3] D.L. Baulch, C.T. Bowman, C.J. Cobos, R.A. Cox, T. Just, J.A. Kerr, M.J. Pilling, D. Stocker, J. Troe, W. Tsang, R.W. Walker, J. Warnatz, J. Phys. Chem. Ref. Data 34 (2005) in press.

[4] D.L. Baulch, C.J. Cobos, R.A. Cox, P. Frank, G. Hayman, T. Just, J.A. Kerr, T. Murrells, M.J. Pilling, J. Troe, R.W. Walker, J. Warnatz, J. Phys. Chem. Ref. Data 23 (1994) 847.
[5] D.L. Baulch, C.J. Cobos, R.A. Cox, C. Esser, P. Frank, T. Just, J.A. Kerr, M.J. Pilling, J. Troe, R.W. Walker, J. Warnatz, J. Phys. Chem. Ref. Data 21 (1992) 411.
[6] A.I. Fernandez, A.A. Viggiano, T.M. Miller, S. Williams, I. Dotan, J.V. Seeley, J. Troe, J. Phys. Chem. A 108 (2004) 9652.
[7] J. Troe, A.A. Viggiano, S. Williams, J. Phys. Chem. A 108 (2004) 1574.
[8] A.A. Viggiano, T.M. Miller, S. Williams, S.T. Arnold, J.V. Seeley, J.F. Friedman, J. Phys. Chem. A 106 (2002) 11917.
[9] S. Williams, A.J. Midey, S.T. Arnold, R.A. Morris, A.A. Viggiano, Y.-H. Chiu, D.J. Levandier, R.A. Dressler, M.R. Berman, J. Phys. Chem. A 104 (2000) 10336.
[10] S.T. Arnold, J.V. Seeley, J.S. Williamson, P.L. Mundis, A.A. Viggiano, J. Phys. Chem. A 104 (2000) 5511.
[11] S.T. Arnold, A.A. Viggiano, J. Phys. Chem. A 105 (2001) 3527.
[12] T.D. Fridgen, T.B. McMahon, J. Troe, A.A. Viggiano, A.J. Midey, S. Williams, J. Phys. Chem. A 108 (2004) 5600.
[13] J. Troe, V.G. Ushakov, A.A. Viggiano, J. Chem. Phys. 122 (2005) in press.
[14] J. Troe, J. Phys. Chem. 83 (1979) 114.
[15] S. Hamon, T. Speck, J.B.A. Mitchell, B.R. Rowe, J. Troe, J. Chem. Phys. 117 (2002) 2557.
[16] J. Troe, J. Phys. Chem. Chem. Phys. 7 (2005) in press.
[17] U. Hueter, Creating an airline to the stars, in Aerospace America, 1999, p. 40.
[18] E.T. Curran, J. Propulsion and Power 17 (2001) 1138.
[19] O.A. Powell, J.T. Edwards, R.B. Norris, K.E. Numbers, J.A. Pearce, J. Propulsion and Power 17 (2001) 1170.
[20] T., Edwards, M.L. Meyer. Propellant requirements for future aerospace propulsion systems, in: Proceedings of the AIAA 2002-3870, 38th AIAA/ASME/SAE/ASEE Joint Propulsion Conference and Exhibit, 2002, Indianapolis, Indiana.
[21] T., Edwards. 'Kerosene' fuels for aerospace propulsion-composition and properties, in: Proceedings of the AIAA 2002-3874, 38th AIAA/ASME/SAE/ASEE Joint Propulsion Conference and Exhibit, 2002, Indianapolis, Indiana.
[22] S. Williams, S.T. Arnold, P.M. Bench, A.A. Viggiano, I. Dotan, A.J. Midey, T. Morris, R.A. Morris, L.Q. Maurice, E.A. Sutton, Potential enhancement of hydrocarbon fueled combustor performance via ionization, in: Proceedings of the ISABE 99-7236, 14th International Symposium on Air Breathing Engines, 1999, Florence, Italy.
[23] S. Williams, A.J. Midey, S.T. Arnold, P.M. Bench, A.A. Viggiano, R.A. Morris, L.Q. Maurice, C.D. Carter, Progress on the investigation of the effects of ionization on hydrocarbon/air combustion chemistry, in: Proceedings of the AIAA 99-4907, 9th International Space Planes and Hypersonic Systems and Technologies Conference, 1999, Norfolk, VA.
[24] S. Williams, S. Popovic, L. Vuskovic, C. Carter, L. Jacobson, S. Kuo, D. Bivolaru, S. Corera, M. Kahandawala, S. Sidhu, Model and igniter development for plasma assisted combustion, in: Proceedings of the AIAA 2004-1012, 42nd Aerospace Sciences Meeting and Exhibit, 2004, Reno, Nevada.
[25] T. Nagashima, H. Kitamura, S. Obata, Supersonic combustion of hydrogen in tandem transverse injection with oxygen radicals, in: SABE Paper 97-7055, Proceedings of the XIII International Symposium on Air Breathing Engines (ISABE), 1997, Chattanooga, TN.
[26] T. Mathur, G. Streby, M. Gruber, K. Jackson, J. Donbar, W. Donaldson, T. Jackson, C. Smith, F. Billig, Supersonic combustion experiments with a cavity-based fuel injector, in: Proceedings of the AIAA 99-2102, 35th AIAA/ASME/SAE/ASEE Joint Propulsion Conference and Exhibit, 1999, Los Angeles, CA.
[27] M.R. Gruber, R.A. Baurle, T. Mathur, K.-Y. Hsu, Fundamental studies of cavity-based flameholder concepts for supersonic combustors, in: Proceedings of the AIAA 99-2248, 35th AIAA/ASME/SAE/ASEE Joint Propulsion Conference and Exhibit, 1999, Los Angeles, CA.
[28] T. Edwards, L.Q. Maurice, J. Propulsion Power 17 (2001) 461.
[29] M.A. Mawid, T.W. Park, B. Sekar, C. Arana, Sensitivity of JP-8 fuel combustion and ignition to aromatic compounds, in: Proceedings of the AIAA 2003-4938, 39th AIAA/ASME/SAE/ASEE Joint Propulsion Conference and Exhibit, 2003, Huntsville, Alabama.
[30] M.A. Mawid, T.W. Park, B. Sekar, C. Arana, Importance of surrogate JP-8/Jet-A fuel composition in detailed chemical kinetics development, in: Proceedings of the AIAA 2004-4207, 40th AIAA/ASME/SAE/ASEE Joint Propulsion Conference and Exhibit, 2004, Fort Lauderdale, Florida.
[31] S. Williams, A.J. Midey, S.T. Arnold, T.M. Miller, P.M. Bench, R.A. Dressler, Y.-H. Chiu, D.J. Levandier, A.A. Viggiano, R.A. Morris, M.R. Berman, L.Q. Maurice, C.D. Carter, Progress on the investigation of the effects of ionization on hydrocarbon/air combustion chemistry: kinetics and thermodynamics of C6-C10 hydrocarbon ions, in: Proceedings of the AIAA 2001-28734th Weakly Ionized Gases Workshop, 2001, Anaheim, California.
[32] E.D. Hausmann, C.J. King, Ind. Eng. Chem. Fund. 5 (1966) 295.
[33] C.T. Brooks, S.J. Peacock, B.G. Reuben, J. Chem. Soc. Faraday Trans. 1 (78) (1982) 3187.
[34] A.J. Midey, S. Williams, S.T. Arnold, A.A. Viggiano, J. Phys. Chem. A 106 (2002) 11726.
[35] S.T. Arnold, I. Dotan, S. Williams, A.A. Viggiano, R.A. Morris, J. Phys. Chem. A 104 (2000) 928.
[36] Y.H. Kim, J.C. Choe, M.S. Kim, J. Phys. Chem. A 105 (2001) 5751.
[37] M. Malow, M. Penno, K.-M. Weitzel, J. Phys. Chem. 107 (2003) 10625.
[38] W.G. Hwang, J.H. Moon, J.C. Choe, M.S. Kim, J. Phys. Chem. A. 102 (1998) 7512.
[39] W.J. Chesnavich, M.T. Bowers, J. Chem. Phys. 66 (1977) 2306.
[40] W.J. Chesnavich, M.T. Bowers, J. Am. Chem. Soc. 99 (1977) 1705.
[41] C.J. Cobos, J. Troe, J. Chem. Phys. 83 (1985) 1010.
[42] T. Su, W.J. Chesnavich, J. Chem. Phys. 76 (1982) 5183.
[43] J. Troe, J. Chem. Phys. 66 (1977) 4745.
[44] J. Troe, Chem. Phys. 190 (1995) 381.
[45] J. Troe, V.G. Ushakov, Faraday Discuss. 119 (2001) 145.
[46] J. Troe, Ber. Bunsen.-Ges. Phys. Chem. 87 (1983) 161.
[47] R.G. Gilbert, K. Luther, J. Troe, Ber. Bunsen.-Ges. Phys. Chem. 87 (1983) 169.